Bandwidth limitations for scattering of higher order electromagnetic spherical waves with implications for the antenna scattering matrix

Bernland, Anders

2011

CODEN:LUTEDX/(TEAT-7214)/1-23/(2011)

Revision No. 1: March 2012

Bandwidth limitations for scattering of higher order electromagnetic spherical waves with implications for the antenna scattering matrix

Anders Bernland

Electromagnetic Theory
Department of Electrical and Information Technology
Lund University
Sweden

Anders Bernland
Anders.Bernland@eit.lth.se

Department of Electrical and Information Technology
Electromagnetic Theory
Lund University
P.O. Box 118
SE-221 00 Lund
Sweden

Editor: Gerhard Kristensson

Abstract

Various physical limitations in electromagnetic theory and antenna theory have received considerable attention recently. However, there are no previous limitations on the scattering of higher order electromagnetic vector spherical waves, despite the widespread use of spherical wave decompositions. In the present paper, bandwidth limitations on the scattering matrix are derived for a wide class of heterogeneous objects, in terms of their electrical size, shape and static material properties. In particular, it is seen that the order of the dominating term in the Rayleigh limit increases with the order of the spherical wave. Furthermore, it is shown how the limitations place bounds on the antenna scattering matrix, thus introducing a new approach to physical limitations on antennas. Comparisons to other types of antenna limitations are given, and numerical simulations for two folded spherical helix antennas and a directive Yagi-Uda antenna are included to illuminate and validate the theory. The results in this paper are derived using a general approach to derive limitations for passive systems: First, the low-frequency asymptotic expansion of the scattering matrix of a general scatterer is derived. This gives a set of sum rules, from which the limitations follow.

1 Introduction

Scattering of electromagnetic waves is essential to a wide range of applications, from classical optics to wireless communication and radar. In many cases it is beneficial to decompose the fields in electromagnetic vector spherical waves [28] (also referred to as partial waves, TM- and TE-modes or electric and magnetic multipoles). For instance, spherical waves are used for analysing scattering by spherical particles (Mie theory) [6], in Waterman's T-matrix method [27], in antenna measurements [19], and recently also for modelling wireless communication channels [12].

In the last few years, there has been an interest in physical limitations for electromagnetic scattering; several interesting attempts have been made to quantify the intuitively obvious statement that objects which are small compared to the wavelength can only provide limited interaction with electromagnetic waves [35]. Specific issues addressed are e.g. radar absorbers [32], high-impedance surfaces [8, 18] and metamaterials [13]. Various antenna limitations have received considerable attention recently (a review can be found in the book by Volakis et al. [39]). Despite the widespread use of spherical wave decompositions, however, there are no previous limitations on higher order spherical wave scattering.

The main results of the present paper are improved limitations for scattering of higher order electromagnetic vector spherical waves (quadrupoles, octopoles and so forth), originally derived for the dipole case in [3]. The limitations imply that the diagonal elements of the scattering matrix, which relates the coefficients of the incoming and outgoing waves, cannot be arbitrarily small over a whole wavelength interval; the bound depends on the fractional bandwidth as well as the size, shape and static material properties of the scatterer.

The results of this paper pave the way for a new approach to physical limitations

on antennas. In form, the sum rules and limitations derived here are similar to those from optimal broadband matching of the spherical waves. Matching of ideal dipoles, the lowest order spherical waves, was considered by Hujanen et al. [21], while higher order waves was treated by Villalobos et al. [38], Nordebo et al. [29], as well as Kogan (see [24] and references therein). One advantage that follows from the approach adopted in the present paper is that the shape and static material properties of the antenna are highlighted. Many previous publications on antenna limitations were concerned with the quality factors (Q-factors) of the spherical waves, but it is in general not straightforward to relate the Q-factor to the operating bandwidth of the antenna [16, 36]. Recently, a different method, based on sum rules for the extinction cross section, has been proposed by Gustafsson et al. [14, 15, 34]. Unfortunately, these results cannot handle antennas placed in a dielectric background or spherical wave decompositions. Spherical waves are a useful tool e.g. for analysing multiple-input multiple-output (MIMO) antenna systems [12, 17, 26].

The derivations in this paper follow a general approach to achieve sum rules and physical limitations for passive systems presented in [4], cf. also [3, 29]. It relies on the well-known connection between passive systems and Herglotz (or positive real) functions [43, 44] in conjunction with a set of integral identities for that class of functions. To use the approach, an intermediate result needs to be derived in the paper: the low-frequency asymptotic expansion of the scattering matrix of a general scatterer.

The outline of the paper is the following: Section 2 introduces the scattering and transition matrices as well as the electromagnetic vector spherical waves. Their low-frequency asymptotic expansions and static counterparts are also covered. The sum rules and limitations for the scattering matrix are derived in Section 3. Implications for the antenna scattering matrix are given in Section 4, and the results are compared to the broadband matching limitations. Simulation results for two folded spherical helix antennas and a directive Yagi-Uda antenna are also presented. Section 5 concludes the paper.

2 The scattering and transition matrices

This section presents the scattering problem considered in this paper. It is described in terms of vector spherical waves and the scattering and transition matrices, which are introduced in Section 2.1. Time-harmonic fields and sources are considered throughout this paper, and the time convention $\mathrm{e}^{-\mathrm{i}\omega t}$, where i is the imaginary unit and ω is the angular frequency, is used. The low-frequency and static cases, which are essential to the further analysis in later sections, are treated in Section 2.2.

2.1 Scattering geometry

Consider an uncharged scatterer in free space. Let the scatterer be contained in a hypothetical sphere of radius a, centered at the origin, as in Figure 1. The electric and magnetic fields can be written as sums of incoming ($\boldsymbol{u}^{(2)}$) and outgoing ($\boldsymbol{u}^{(1)}$)

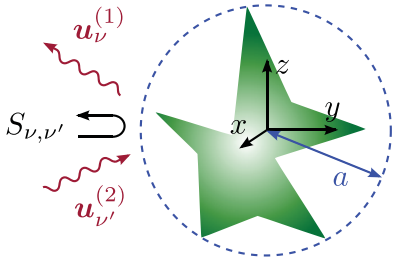

Figure 1: The scatterer is placed in free space and circumscribed by a hypothetical sphere of radius a, centered at the origin. The electric and magnetic fields are written as sums of incoming ($\boldsymbol{u}_\nu^{(2)}$) and outgoing ($\boldsymbol{u}_\nu^{(1)}$) electromagnetic vector spherical waves, with index ν, outside the sphere. The scattering matrix $\mathbf{S}$, with elements $S_{\nu,\nu'}$, relates the coefficients of the incoming and outgoing waves.

vector spherical waves outside the circumscribing sphere [28]. The scattering matrix $\mathbf{S}$ relates the coefficients of the incoming and outgoing waves, and is thus a measure on the incoming power that is rejected by the scatterer.

The spherical wave decomposition of the electric and magnetic fields outside the circumscribing sphere is [28]

$$\boldsymbol{E}(\boldsymbol{r},k) = k\sqrt{2\eta_0}\sum_\nu b_\nu^{(1)}\boldsymbol{u}_\nu^{(1)}(k\boldsymbol{r}) + b_\nu^{(2)}\boldsymbol{u}_\nu^{(2)}(k\boldsymbol{r}). \tag{2.1}$$

Here the free space parameters are wavenumber $k = \omega/\mathrm{c}$, speed of light c and impedance η_0. The spatial coordinate is denoted $\boldsymbol{r}$, with $r = |\boldsymbol{r}|$ and $\hat{\boldsymbol{r}} = \boldsymbol{r}/r$. The vector spherical waves are defined as in [7], see Appendix A. The multi-index $\nu = 2(l^2 + l - 1 + (-1)^s m) + \tau$ is introduced in place of the indices $\{\tau, s, m, l\}$ to simplify the notation. It is defined so that $\tau = 1$ (odd ν) corresponds to a magnetic 2^l-pole (TE$_l$-mode), while $\tau = 2$ (even ν) identifies an electric 2^l-pole (TM$_l$-mode). Hence, $l = 1$ denotes dipoles, $l = 2$ quadrupoles, and so on. The corresponding magnetic field is $\boldsymbol{H}(\boldsymbol{r},k) = \frac{1}{\mathrm{i}k\eta_0}\nabla \times \boldsymbol{E}(\boldsymbol{r},k)$. With this normalization, the time-average of the power passing out through a sphere of radius $r > a$ is

$$\langle P(t)\rangle = \int_{\Omega_{\hat{\boldsymbol{r}}}} \hat{\boldsymbol{r}} \cdot \mathrm{Re}\left(\frac{1}{2}\boldsymbol{E}(\boldsymbol{r},k) \times \boldsymbol{H}^*(\boldsymbol{r},k)\right) r^2 \,\mathrm{d}\Omega_{\hat{\boldsymbol{r}}} = \sum_\nu |b_\nu^{(1)}|^2 - |b_\nu^{(2)}|^2, \tag{2.2}$$

where $\Omega_{\hat{\boldsymbol{r}}} = \{(\theta,\phi) : 0 \le \theta < \pi, 0 \le \phi < 2\pi\}$ is the unit sphere and $\mathrm{d}\Omega_{\hat{\boldsymbol{r}}} = \sin\theta \,\mathrm{d}\theta \,\mathrm{d}\phi$.

Alternatively, the fields can be decomposed into outgoing and regular waves $\boldsymbol{v}_\nu$:

$$\boldsymbol{E}(\boldsymbol{r},k) = k\sqrt{2\eta_0}\sum_\nu d_\nu^{(1)}\boldsymbol{u}_\nu^{(1)}(k\boldsymbol{r}) + d_\nu^{(2)}\boldsymbol{v}_\nu(k\boldsymbol{r}). \tag{2.3}$$

An incident field is regular at the origin, and so constitutes the sum over the regular waves, while the scattered field makes up the sum over the outgoing waves in (2.3).

The infinite dimensional scattering matrix $\mathbf{S}$ relates the coefficients in (2.1): $b_\nu^{(1)} = \sum_{\nu'} S_{\nu,\nu'} b_{\nu'}^{(2)}$. The counterpart for (2.3) is the transition matrix $\mathbf{T}$: $d_\nu^{(1)} =$

$\sum_{\nu'} T_{\nu,\nu'} d^{(2)}_{\nu'}$. The scattering and transition matrices are related as $\mathbf{S} = 2\mathbf{T} + \mathbf{I}$, where $\mathbf{I}$ is the infinite dimensional identity matrix. Note that it has now been implicitly assumed that the constitutive relations of the scatterer are in convolution form in the time domain [3]. The convolution form assumption is closely related to the assumptions of linearity and time-translational invariance [44], and is commonly used.

The main results of this paper are limitations for the diagonal elements $S_{\nu,\nu}$ of the scattering matrix. A general approach to derive sum rules and physical limitations for passive systems presented in [4] is used, cf. also [3, 29]. In order to use it, expressions for the low-frequency asymptotic expansions of the scattering and transition matrix elements are required, and this is the topic of Section 2.2.

2.2 Low-frequency asymptotics and statics

The low-frequency and static transition matrices have been considered by a number of authors. Peterson [31] introduced the transition matrices of the static field problem, and noted that it is the low-frequency limit of the dynamic scattering problem. Waterman showed how the electric and magnetic components decouple in the static limit [42], and Olsson treated the elastodynamic case similarly [30]. Recently, Waterman has derived expressions for the low-frequency electromagnetic transition matrix in two dimensions [40] and the acoustic counterpart in three dimensions [41]. A review of results on low-frequency approximations until 2006 can be found in the book by Martin [25]. However, none of these previous publications provides the necessary expressions for the scattering problem considered here.

To be able to derive the required low-frequency asymptotic expansions of the scattering and transition matrix elements, consider a static electric field $\boldsymbol{E}$. The electric field is given by the electrostatic potential, $\boldsymbol{E} = -\nabla\phi$, and the potential can be expanded in scalar spherical harmonics Y_{sml} (defined in (A.3)) [28, 42]:

$$\phi(\boldsymbol{r}) = \sum_{l=0}^{\infty} \sum_{m=0}^{l} \sum_{s=1}^{2} f^{(1)}_{sml} r^{-l-1} Y_{sml}(\hat{\boldsymbol{r}}) - f^{(2)}_{sml} r^{l} Y_{sml}(\hat{\boldsymbol{r}}). \tag{2.4}$$

In this case, the electrostatic transition matrix $\mathbf{T}^{[2]}$ relates the coefficients: $f^{(1)}_{sml} = \sum_{s'm'l'} T^{[2]}_{sml,s'm'l'} f^{(2)}_{s'm'l'}$, cf. [31, 42]. The magnetostatic transition matrix $\mathbf{T}^{[1]}$ is defined analogously; since $\nabla \times \boldsymbol{H} = \boldsymbol{0}$ outside the circumscribing sphere, a magnetostatic scalar potential ϕ^{MS} can be defined there such that $\boldsymbol{H} = -\nabla\phi^{\mathrm{MS}}$. Note that an applied external potential is regular at the origin and constitutes the sum over the terms $f^{(2)}_{sml} r^{l} Y_{sml}(\hat{\boldsymbol{r}})$, while the scattered potential decays at infinity and thus is given by the terms $f^{(1)}_{sml} r^{-l-1} Y_{sml}(\hat{\boldsymbol{r}})$.

To obtain expressions for the low-frequency expansions of the electrodynamic transition matrix, consider the asymptotic expansions of the spherical waves (which follow from the asymptotic expansions for the spherical Bessel and Hankel functions

[2] appearing in their definitions, and some algebra, see Appendix A.1):

$$\begin{aligned}\boldsymbol{v}_{2sml} &= \frac{2^l(l+1)!}{(2l+1)!}\frac{\nabla(r^l Y_{sml}(\hat{\boldsymbol{r}}))}{\sqrt{l(l+1)}}k^{l-1} + \mathcal{O}(k^{l+1}) \\ \boldsymbol{u}^{(1)}_{2sml} &= \frac{\mathrm{i}(2l)!}{2^l(l-1)!}\frac{\nabla(r^{-l-1} Y_{sml}(\hat{\boldsymbol{r}}))}{\sqrt{l(l+1)}}k^{-l-2} + \mathcal{O}(k^{-l}),\end{aligned} \tag{2.5}$$

while $\boldsymbol{v}_{1sml} = \mathcal{O}(k^l)$ and $\boldsymbol{u}^{(1)}_{1sml} = \mathcal{O}(k^{-l-1})$, as $k \to 0$. For the electric case ($\tau = 2$), combining (2.5) with (2.3) and (2.4) readily yields

$$T_{\nu,\nu'} = \frac{\mathrm{i}2^{l+l'}(l-1)!(l'+1)!\sqrt{l(l+1)}}{(2l)!(2l'+1)!\sqrt{l'(l'+1)}}\delta_{\tau,\tau'}T^{[\tau]}_{sml,s'm'l'}k^{l+l'+1} + \mathcal{O}(k^{l+l'+3}) \quad \text{as } k \to 0. \tag{2.6}$$

Here $\delta_{\tau,\tau'}$ is the Kronecker delta. The same equation holds also for the magnetic case ($\tau = 1$), which is seen by also making use of $\boldsymbol{H} = \frac{1}{\mathrm{i}k\eta_0}\nabla \times \boldsymbol{E}$ and (A.1). Recall that the multi-index ν represents the indices $\{\tau, s, m, l\}$.

Equation (2.6), which is needed in the following section in order to derive the limitations for the scattering matrix, cannot be found in any previous publication. The equation explicitly shows how the electrostatic and magnetostatic transition matrices are the low-frequency limits of the electrodynamic counterpart, cf. [42]. Consequently, the static transition matrices are crucial to the limitations. For dipoles ($l = l' = 1$), the elements of $\mathbf{T}^{[2]}$ and $\mathbf{T}^{[1]}$ for an uncharged body are (apart from normalization) equal to the elements of the well-studied static electric and magnetic polarizability dyadics, defined in [23]. The elements of $\mathbf{T}^{[2]}$ and $\mathbf{T}^{[1]}$ for higher order spherical waves can be seen as generalizations of the polarizability dyadics in spherical coordinates, see Appendix B for details.

3 Sum rules and limitations for the scattering matrix

The limitations on the scattering matrix, which are the main results of the paper, are derived in this section. First, in Section 3.1, it is shown that the low-frequency expansion (2.6) implies that a set of sum rules, or integral identities, apply. The sum rules, in turn, are used to obtain the limitations, or inequalities. Similarly as in the case of optimal broadband matching [29, 38], the limitations presented in this paper make up an optimization problem. Its solution is discussed briefly. After that, physical interpretations are given in Section 3.2. Further discussion on interpretations for antennas is given later in Section 4.

3.1 Results

As mentioned in the introduction, the derivations in the present paper rely on a general approach presented in [4] for deriving sum rules and limitations on passive

systems. The approach relies on the connection between passive systems and Herglotz (or positive real) functions [43, 44], and it can be used here since $\mathrm{e}^{\mathrm{i}2ka}S_{\nu,\nu'}(k)$ is a passive reflection coefficient corresponding to a real-valued and causal convolution kernel, under the assumption that the material of the scatterer is passive [3]. The limitations for scattering of dipoles were derived previously in [3], whereas [29] derives matching limitations by relating the matching problem to scattering of spherical waves by a high-contrast sphere (with infinite static relative permeability and permittivity). Both these references contain more mathematical background, and the interested reader is referred there.

The following low-frequency expansion of the diagonal elements of the scattering matrix is required:

$$-\mathrm{i}\log(\mathrm{e}^{\mathrm{i}2ka}S_{\nu,\nu}) = 2ka + 2k^{2l+1}c_l T^{[\tau]}_{sml,sml} + \mathcal{O}(k^{2l+3}), \quad \text{as } k \to 0, \tag{3.1}$$

where $c_l = [2^{2l}(l+1)!(l-1)!]/[(2l+1)!(2l)!]$ is a constant. The equation (3.1) is a straightforward consequence of the low-frequency expansion (2.6) for the transition matrix $\mathbf{T}$, the relation $\mathbf{S} = 2\mathbf{T} + \mathbf{I}$ and the asymptotic expansion $\log(1+z) = z + \mathcal{O}(z^2)$ as $z \to 0$. The off-diagonal elements of $\mathbf{S}$ tend to zero as $k \to 0$, and so the logarithms of them are not well-behaved in the low-frequency limit. For this reason, only the diagonal elements are considered from now on.

Following (3.1), $l+1$ sum rules can be derived [3]:

$$\begin{cases} \frac{1}{\pi}\int_0^\infty \frac{1}{k^2}\ln\frac{1}{|S_{\nu,\nu}(k)|}\,\mathrm{d}k & = a - \frac{\beta_{\nu,\nu}}{2} + \sum_n \operatorname{Im}\frac{1}{k_n} \\ \frac{1}{\pi}\int_0^\infty \frac{1}{k^{2p}}\ln\frac{1}{|S_{\nu,\nu}(k)|}\,\mathrm{d}k & = \frac{1}{2p-1}\sum_n \operatorname{Im}\frac{1}{k_n^{2p-1}}, \quad \text{for } p = 2,3,\ldots,l \\ \frac{1}{\pi}\int_0^\infty \frac{1}{k^{2l+2}}\ln\frac{1}{|S_{\nu,\nu}(k)|}\,\mathrm{d}k & = c_l T^{[\tau]}_{sml,sml} + \frac{1}{2l+1}\sum_n \operatorname{Im}\frac{1}{k_n^{2l+1}}, \end{cases} \tag{3.2}$$

where k_n are the zeros of $S_{\nu,\nu}(k)$ in the open upper half of the complex plane ($\operatorname{Im} k > 0$). The parameter $\beta_{\nu,\nu} \geq 0$ is expected to be zero if the circumscribing sphere is chosen as small as possible [29]. Note the close likeness to Fano's matching equations [11]. In [3], the asymptotic expansion (3.1) was only derived to order k^3, and hence only 2 sum rules were available in (3.2). Ref. [29] used the expansion (3.1) to order k^{2l+1}, but only for the simple case of an isotropic sphere.

To derive limitations, consider a finite wavenumber interval $[k_0(1-B/2), k_0(1+B/2)]$, where k_0 is the center wavenumber and B the relative bandwidth. Denote $S_{0,\nu} = \max_{[k_0(1-B/2),k_0(1+B/2)]}|S_{\nu,\nu}(k)|$. The sum rules then give $l+1$ limitations:

$$\begin{cases} \frac{G_1(B)\ln S_{0,\nu}^{-1}}{\pi} & \leq k_0 a + \sum_n \operatorname{Im}\frac{k_0}{k_n} \\ \frac{G_p(B)\ln S_{0,\nu}^{-1}}{\pi} & \leq \frac{1}{2p-1}\sum_n \operatorname{Im}\left(\frac{k_0}{k_n}\right)^{2p-1}, \quad \text{for } p = 2,3,\ldots,l \\ \frac{G_{l+1}(B)\ln S_{0,\nu}^{-1}}{\pi} & \leq k_0^{2l+1} c_l T^{[\tau]}_{sml,sml} + \frac{1}{2l+1}\sum_n \operatorname{Im}\left(\frac{k_0}{k_n}\right)^{2l+1}, \end{cases} \tag{3.3}$$

where the bandwidth factor $G_p(B)$ for $p = 1, 2, \ldots$ is defined by

$$G_p(B) = \int_{1-B/2}^{1+B/2} \frac{1}{x^{2p}}\,\mathrm{d}x = \frac{1}{2p-1}\frac{(1+B/2)^{2p-1} - (1-B/2)^{2p-1}}{(1-B^2/4)^{2p-1}}.$$

Note that $G_p(B) \approx B$ in the narrowband approximation where $B \ll 1$. Furthermore, seeing that $B \leq G_p(B)$ for all $0 \leq B \leq 2$, the inequalities in (3.3) are valid with $G_p(B)$ replaced by B.

Although they place bounds on the scattering matrix rather than the mismatch, the limitations (3.3) are in form similar to the limitations on optimal wideband matching presented in [29, 38]. Note, however, that the last right hand side differs: It includes an element of a static transition matrix $T^{[\tau]}_{sml,sml}$, which describe the shape and static material properties of the scatterer. The limitations (3.3) coincide with the corresponding limitations in [29, 38] in the simple case when the scatterer is a high-contrast sphere, since then $T^{[\tau]}_{sml,sml} = a^{2l+1}$ [37]. This fact was also noted in [29].

The system of inequalities suffer from a drawback: they incorporate the unknown zeros k_n of $S_{\nu,\nu}(k)$. However, limitations not containing the zeros can be derived by solving the constrained optimization problem given by (3.3), so that

$$\frac{B \ln S^{-1}_{0,\nu}}{\pi} \leq f_\nu(T^{[\tau]}_{sml,sml}; k_0 a), \tag{3.4}$$

where $f_\nu(T^{[\tau]}_{sml,sml}; k_0 a)$ is the solution to (3.3). For the dipole case ($l = 1$), it is sufficient to consider a single complex zero k_n, which gives the closed form solution [3]:

$$f_\nu(T^{[\tau]}_{sm1,sm1}; k_0 a) = \begin{cases} k_0 a - \sqrt[3]{\iota + \xi} + \sqrt[3]{\iota - \xi} & \text{for } k_0 a \leq \sqrt{\frac{a^3}{c_1 T^{[\tau]}_{sm1,sm1}}} \\ k_0 a & \text{otherwise,} \end{cases}$$

where $\xi = 3(k_0 a - k_0^3 c_1 T^{[\tau]}_{sm1,sm1})/2$ and $\iota = \sqrt{1 + \xi^2}$. For higher order waves, it has been conjectured that l complex zeros are sufficient to obtain an optimal solution [38]. The computationally expensive numerical problem is solved by Villalobos et al. in [38]. Alternatively, Kogan has shown that the solution can be found by solving a polynomial equation of order $2l + 1$, see [24]. However, upper bounds on $f_\nu(T^{[\tau]}_{sml,sml}; k_0 a)$ can be derived by considering a single complex zero also for higher order waves, which gives a problem that is straightforward to solve numerically [29]. For this reason, this procedure is chosen in this paper, and the results can be found in Figure 2. The dominating term for small $k_0 a$ (Rayleigh scattering) is [29]:

$$f_\nu(T^{[\tau]}_{sml,sml}; k_0 a) = \left(g_l + \frac{c_l T^{[\tau]}_{sml,sml}}{a^{2l+1}} \right) k_0^{2l+1} a^{2l+1} + \mathcal{O}(k_0^{2l+3} a^{2l+3}), \tag{3.5}$$

as $k_0 a \to 0$, where the term $g_l > 0$ is given by

$$g_l = - \min_{1 \leq m \leq 2l-1} \frac{1}{2l+1} \frac{\sin\left(m\pi \frac{2l+1}{2l}\right)}{\sin^{2l+1}\left(m\pi \frac{1}{2l}\right)}.$$

Equation (3.5) shows that the order of the dominating term in the Rayleigh regime increases with the order of the spherical wave; something that is also evident from the tangentials of the curves in Figure 2.

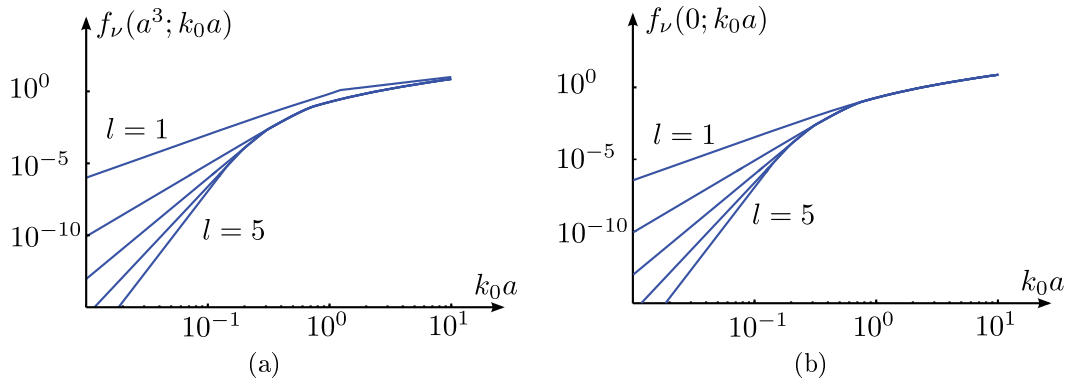

Figure 2: Upper bounds, $B \ln S_{0,\nu}^{-1}/\pi \leq f_\nu(T^{[\tau]}_{sml,sml}; k_0a)$, for $l = 1 \ldots 5$. The bounds are for (a): $T^{[\tau]}_{sml,sml} = a^{2l+1}$ (high-contrast sphere) and (b): $T^{[\tau]}_{sml,sml} = 0$.

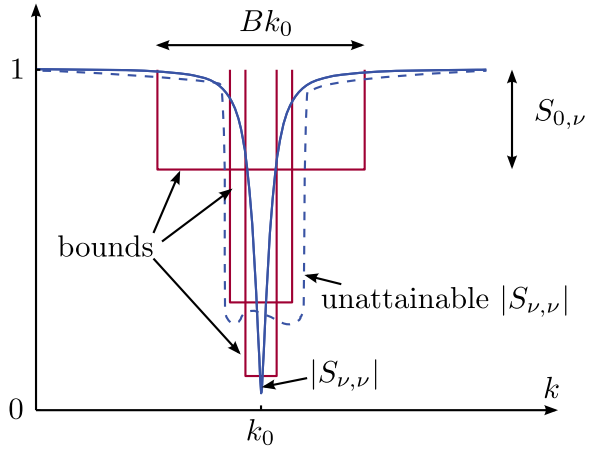

Figure 3: Interpretation of the limitations (3.4). Bounds for a given wave index ν and center wavenumber k_0 are shown for three different values of $S_{0,\nu}$ (and thus three different values of B). The limitations state that $|S_{\nu,\nu}(k)|$ have to intersect the boxes. The figure also shows one attainable and one unattainable element $S_{\nu,\nu}$.

3.2 Physical interpretations

The limitations (3.4) imply that the moduli of the scattering matrix elements $S_{\nu,\nu}$ cannot be arbitrarily small over a whole wavelength interval, see Figure 3. How small they can be is determined by the relative bandwidth B, as well as the electrical size of the scatterer (center wavenumber k_0 times radius a of the circumscribing sphere) and its shape and static material properties (described by the static transition matrix elements $T^{[\tau]}$). Alternatively, any chosen value of $S_{0,\nu} \in [0, 1]$ determines how large the fractional bandwidth B may be.

The absorption efficiency

$$\eta_\nu(k) = 1 - \sum_{\nu'} |S_{\nu',\nu}(k)|^2 \leq 1 - |S_{\nu,\nu}(k)|^2 \tag{3.6}$$

is the relative power of the incoming spherical wave with index ν that is absorbed

by the scatterer [3]. Recall that the off-diagonal terms $S_{\nu',\nu}(k)$ tend to zero as $k \to 0$. The limitations (3.3) imply that $\eta_\nu(k)$ cannot be arbitrarily high over a whole wavelength interval:

$$\min_{[k_0(1-B/2),k_0(1+B/2)]} \eta_\nu(k) \leq 1 - \mathrm{e}^{-2\pi f_\nu(T^{[\tau]}_{sml,sml};k_0a)/B}. \tag{3.7}$$

Many applications concerned with electromagnetic scattering can make use of the limitations (3.4) and (3.7). An example of the limitations (3.7) for the dipole case applied to nanoshells can be found in Section 5.1 in [3].

The static transition matrix elements $T^{[\tau]}_{sml,sml}$ are well understood for dipoles ($l = 1$), see [3] and references therein. The higher order static transition matrix elements are not as well-studied; there are, however, a few previous publications, see [25, 31, 40, 42]. A couple of general remarks can also be made: Firstly, note that the magnetostatic transition matrix $\mathbf{T}^{[1]}$ vanishes when the scatterer is non-magnetic. This gives the upper bounds $f_\nu(0; k_0a)$ in Figure 2b. Secondly, variational principles put forth by Sjöberg in [33] show that $T^{[\tau]}_{sm1,sm1}$ ($l = 1$) is bounded from above by its value for the high-contrast sphere, i.e. $T^{[\tau]}_{sm1,sm1} \leq a^3$. If the same holds also for higher order modes, namely that $T^{[\tau]}_{sml,sml} \leq a^{2l+1}$, it means that the upper bounds $f_\nu(a^{2l+1}; k_0a)$ in Figure 2a are absolute upper bounds. Also recall that for a high contrast sphere, the scattering matrix limitations (3.3) are identical to the broadband matching limitations in [29, 38].

4 Interpretations for antennas

Since the limitations (3.4) can be interpreted as bounds on the absorption of power from each spherical wave, they are well suited to study antennas. More precisely, the limitations have implications for the *antenna scattering matrix*, defined in [19]. This is explained in Section 4.1. Furthermore, it was also mentioned above that the limitations are similar in form to the broadband matching limitations presented in [29, 38]. The interpretations, however, are different, as discussed in Section 4.2. Comparisons to Q-factor and gain-bandwidth limitations are given in Section 4.3. Finally, simulation results for two folded spherical helix antennas (one linearly polarized and the other elliptically polarized) and a directive Yagi-Uda antenna are presented in Section 4.4.

4.1 Limitations on the antenna scattering matrix

Consider an antenna as in Figure 4, connected to a local port through a matching network. The antenna scattering matrix $\mathbf{S}^{\mathrm{A}}$ completely describes the antenna properties:

$$\underbrace{\begin{pmatrix} \Gamma & \mathbf{R}^{\mathrm{A}} \\ \mathbf{T}^{\mathrm{A}} & \mathbf{S} \end{pmatrix}}_{\mathbf{S}^{\mathrm{A}}} \begin{pmatrix} w^{(2)} \\ \boldsymbol{b}^{(2)} \end{pmatrix} = \begin{pmatrix} w^{(1)} \\ \boldsymbol{b}^{(1)} \end{pmatrix}, \tag{4.1}$$

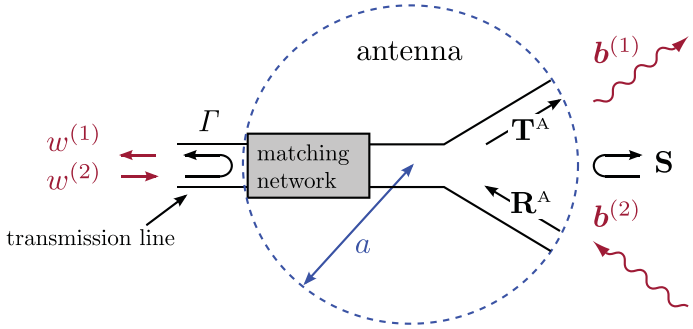

Figure 4: The antenna scattering matrix $\mathbf{S}^{\mathrm{A}}$ in (4.1) completely describes the antenna properties.

Here $\boldsymbol{b}^{(1)} = (b_1^{(1)}\ b_2^{(1)}\ \ldots)^{\mathrm{T}}$ and $w^{(1)}$ are the coefficients of the outgoing waves and received signal, respectively, whereas $\boldsymbol{b}^{(2)} = (b_1^{(2)}\ b_2^{(2)}\ \ldots)^{\mathrm{T}}$ and $w^{(2)}$ are the coefficients of the incoming waves and transmitted signal. The signals are normalized so that their power content is $|w^{(2)}|^2$ and $|w^{(1)}|^2$, respectively. Recall that the spherical waves are normalized similarly, see (2.2). Apart from the scattering matrix $\mathbf{S}$, which describes the scattering properties of the antenna, the antenna scattering matrix $\mathbf{S}^{\mathrm{A}}$ also incorporates the antenna reflection coefficient Γ as well as the transmitting coefficients T_ν^{A} in $\mathbf{T}^{\mathrm{A}}$ and the receiving coefficients R_ν^{A} in $\mathbf{R}^{\mathrm{A}}$ [19]. If the alternative decomposition in (2.3) is used instead of (2.1), equation (4.1) becomes [19]:

$$\begin{pmatrix} \Gamma & \frac{1}{2}\mathbf{R}^{\mathrm{A}} \\ \mathbf{T}^{\mathrm{A}} & \frac{1}{2}(\mathbf{S}-\mathbf{I}) \end{pmatrix} \begin{pmatrix} w^{(2)} \\ \boldsymbol{d}^{(2)} \end{pmatrix} = \begin{pmatrix} w^{(1)} \\ \boldsymbol{d}^{(1)} \end{pmatrix}. \tag{4.2}$$

This is beneficial for use in numerical simulations, see Section 4.4. The antenna scattering matrix can also be generalized for multi-port antennas [17].

The limitations (3.4) place bounds on the antenna scattering matrix. The receiving coefficients R_ν^{A} are evidently bounded by the absorption efficiency η_ν, defined in (3.6):

$$|R_\nu^{\mathrm{A}}| \leq \eta_\nu \leq 1 - |S_{\nu,\nu}|^2. \tag{4.3}$$

The first inequality is an equality for lossless antennas. Consequently, from (3.7) it follows that

$$\min_{[k_0(1-B/2),k_0(1+B/2)]} |R_\nu^{\mathrm{A}}(k)| \leq 1 - \mathrm{e}^{-2\pi f_\nu(T^{[\tau]}_{sml,sml};k_0 a)/B}. \tag{4.4}$$

For reciprocal antennas, the transmitting and receiving coefficients are related as $R_\nu^{\mathrm{A}} = (-1)^s T_\nu^{\mathrm{A}}$ [17] (recall the indices $\{\tau, s, m, l\}$, see Appendix A), and therefore (4.4) applies also with R_ν^{A} replaced by T_ν^{A} in this case.

Consequently, there is an upper bound on the maximum achievable bandwidth of an antenna when it is receiving (or transmitting) a certain spherical wave. As discussed in Section 3.2, the bound depends on the electrical size of the antenna as well as its shape and static material properties. Furthermore, due to (3.5) it is clear that it is increasingly harder to take advantage of the higher order spherical waves for an electrically small antenna. This is also known previously due to the high reactive energies associated with higher order spherical waves [10].

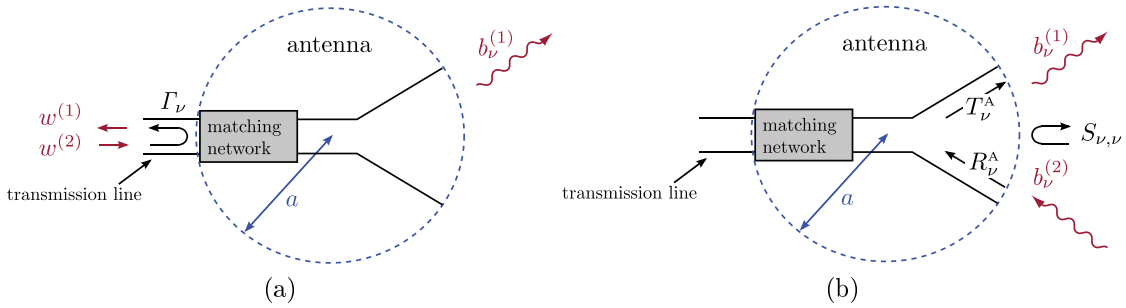

Figure 5: Comparison of the broadband matching limitations presented in [29, 38] and the scattering limitations presented in this paper. (a): The matching limitations place a lower bound on the antenna reflection coefficient Γ_ν when the antenna is designed to transmit a certain spherical wave with index ν. (b): The scattering limitations place lower bounds on the scattering coefficients $S_{\nu,\nu}$ and upper bounds on the antenna receiving and transmitting coefficients R_ν^{A} and T_ν^{A} due to (4.3).

4.2 Comparison to broadband matching limitations

The matching limitations in [29, 38] also place upper bounds on the maximum achievable bandwidth of an antenna receiving or transmitting a certain spherical wave. However, they are not directly comparable to the limitations presented in this paper: The matching limitations place a lower bound on the antenna reflection coefficient Γ_ν when the antenna is transmitting a certain spherical wave with index ν, see Figure 5a. Recall that the limitations (3.4) in this paper instead place lower bounds on the scattering coefficients $S_{\nu,\nu}$ and upper bounds on the antenna receiving and transmitting coefficients R_ν^{A} and T_ν^{A} due to (4.3), see Figure 5b.

One advantage thanks to the approach chosen in the present paper is that the derived limitations highlight the shape and static material properties of the antenna, and not just its electrical size as in [29, 38]. This can lead to sharper bounds in some cases. If, for instance, the antenna is non-magnetic, the bounds for the magnetic spherical waves (TE-modes) are sharpened since the magnetostatic transition matrix $\mathbf{T}^{[1]}$ vanishes. Recall, though, that the limitations (3.4) coincide with the corresponding limitations in [29, 38] for the simple case of a high contrast sphere. Another advantage of the scattering approach to antenna limitations is that it is directly applicable to other areas concerned with electromagnetic scattering, as discussed in Section 3.2 and [3].

4.3 Comparisons to Q-factor and gain-bandwidth limitations

It is hard to make a direct comparison between the scattering (or matching) limitations for spherical waves with other bounds on antennas, but is still worthwhile to make a consistency check. The various approaches reach different conclusions, and should therefore be considered as complementary rather than in competition; there is not one approach that reaches the best result for every case.

Lower bounds on the Q-factor were first presented by Chu in [9], and closed

form expressions for higher order waves were derived by Collin and Rothschild, see equation (10) in [10]. Even though there is no general relationship between Q-factor and bandwidth, for many antennas it can be argued that $B \ln \Gamma_0^{-1}/\pi \leq 1/Q$, where $\Gamma_0 = \max_{[k_0(1-B/2),k_0(1+B/2)]} |\Gamma(k)|$ [16]. Hence the upper bounds on $1/Q$ in [10] are on equal footing to the upper bounds on f_ν in (3.4) and Figure 2. A closer comparison reveals that the numerical values are comparable for a high-contrast sphere, and the Q-bounds also show the same asymptotic behaviour for small $k_0 a$. For $l = 1$, the results are almost identical, whereas the Q-bounds are better for $l > 1$; this is probably due to the simplified optimization procedure adopted in this paper, see Section 3.1. However, the results in [10] do not take shape and material properties into account, as do (3.4).

Bounds on gain and bandwidth were derived by Gustafsson et al. using sum rules for the extinction cross section, see equation (3.4) in [14]. Inserting the directivity of a spherical wave ($D = 1.5$ for $l = 1$, $D = 2.5$ for $l = 2$, and so fort) yields an upper bound on $B(1 - \Gamma_0^2)$, which can be compared to (3.4). The numerical values are comparable for electric dipoles ($\tau = 2, l = 1$) and non-magnetic materials; the bounds in (3.4) are slightly sharper for narrow bandwidths, and the other way around for wider bandwidths. The results in [14] *do* take shape and material properties into account (in terms of the static polarizability dyadics), and provide sharper bounds for non-spherical circumscribing geometries. However, the results presented in this paper provide sharper bounds for the case of electric dipoles *with* magnetic materials, magnetic dipoles *without* magnetic materials, as well as for higher order waves ($l > 1$).

4.4 Numerical examples

To illustrate the limitations (3.4) and (4.4), two folded spherical helix antenna designs proposed by Best [5] have been considered. These designs were chosen since their quality factors are close to the Chu-bound [5]. Both antennas fit into a sphere of radius $a = 4.18\,\text{cm}$. The first design is linearly polarized, and it turns out that the spherical wave with multi-index $\nu = 4$ (i.e. $\{\tau, s, m, l\} = \{2, 2, 0, 1\}$) is dominant. This corresponds to an electric dipole (TM_1-mode) in the $z-$direction. The antenna geometry, scattering matrix element $S_{4,4}$, reflection coefficient Γ, and transmitting and receiving coefficients T_4^{A} and R_4^{A} are depicted in Figure 6 along with the limitations. The second design is elliptically polarized, and it radiates two spherical waves: the electric dipole with multi-index $\nu = 4$, and the magnetic dipole (TE_1-mode) in the $z-$direction with multi-index $\nu = 3$ (i.e. $\{\tau, s, m, l\} = \{1, 2, 0, 1\}$). The results can be found in Figure 7. Note that the limitations are sharper for the magnetic dipole, since the magnetostatic transition matrix $T^{[1]}$ vanishes for a non-magnetic antenna. It can be seen that both spherical helices approach the limitations (3.4) and (4.4).

An antenna with directivity greater than 3 must have a radiation pattern that includes spherical waves of orders higher than dipoles, since an antenna radiating only dipole modes must have directivity $D \leq 3$ [20]. As a consequence of the limitations (3.4), such an antenna must be narrowband and/or electrically large.

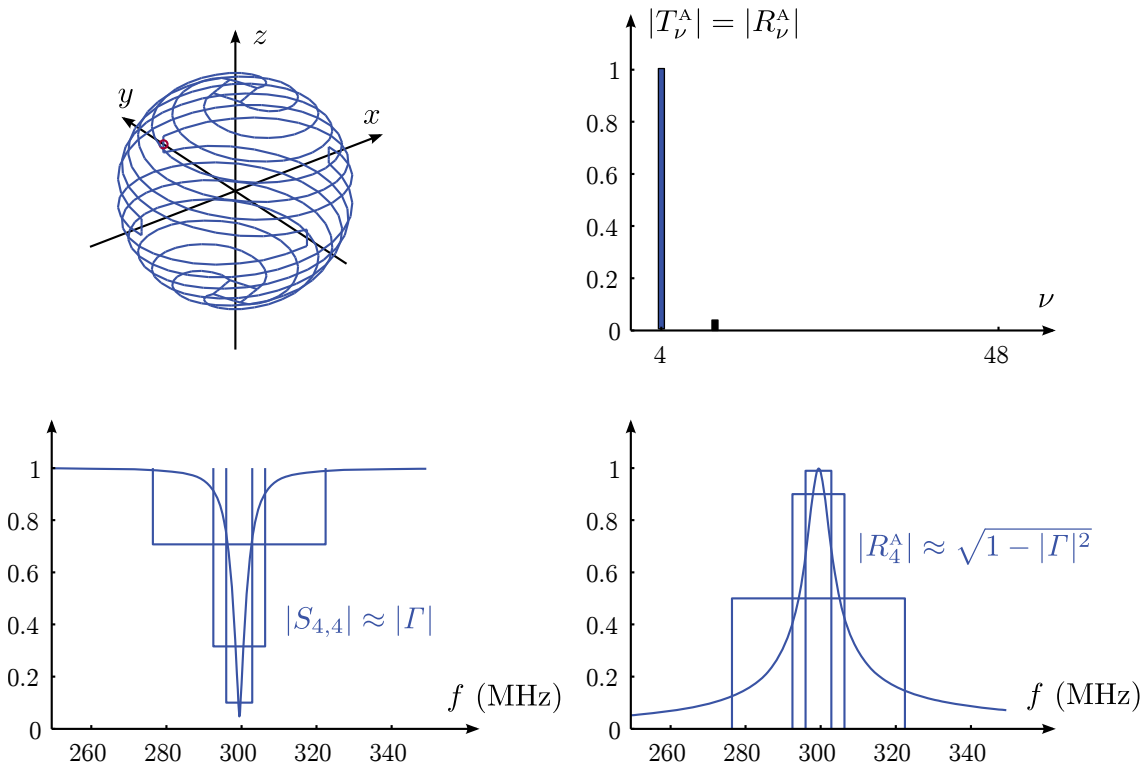

Figure 6: Upper left: The geometry of the linearly polarized folded spherical helix (the red circle marks the location of the feed). Upper right: The moduli of the transmitting and receiving coefficients, $|T_\nu^{\mathrm{A}}| = |R_\nu^{\mathrm{A}}|$, at the resonance frequency $f = 299\,\mathrm{MHz}$. Lower left: Reflection coefficient Γ and scattering matrix element $S_{4,4}$ with the bound (3.4) for three different values of $S_{0,\nu}$. Lower right: Square root of the mismatch $(1 - |\Gamma|^2)$, and receiving coefficient R_4^{A} with the bound (4.4).

A design of a directive Yagi-Uda antenna recently proposed by Arceo and Balanis in [1] has been simulated here (the specific dimensions labelled "C" in Table I in [1] was used). It has a maximum directivity of $D = 5.7$, and the results for the antenna scattering matrix can be found in Figure 8. It is seen that there are three dominating modes: $\nu = 1$ (magnetic dipole), $\nu = 4$ (electric dipole), and $\nu = 14$ (electric quadrupole). This antenna is electrically large, (it has $k_0 a = 1.42$), and therefore the numerical values of the limitations (3.4) do not give much useful information and are not included in the figure. The design of an electrically small antenna that approaches the limitations (3.4) for higher order modes is an open problem.

It should be noted that the simulation results in this paper do not perfectly match those from the references [5] and [1]. One reason is that the exact dimensions of the antennas were not clear. Another is that the wires were modelled as perfectly conducting in this paper (the wire diameter is 2.6 mm for the spherical helices and 3.0 mm for the Yagi-Uda), whereas the simulations and measurements in the references are for realistic material parameters. Lastly, the Yagi-Uda antenna was modelled as a dipole in this paper, rather than as a monopole over a ground plane. However, the task was not to verify the results of the references, but to pick clever

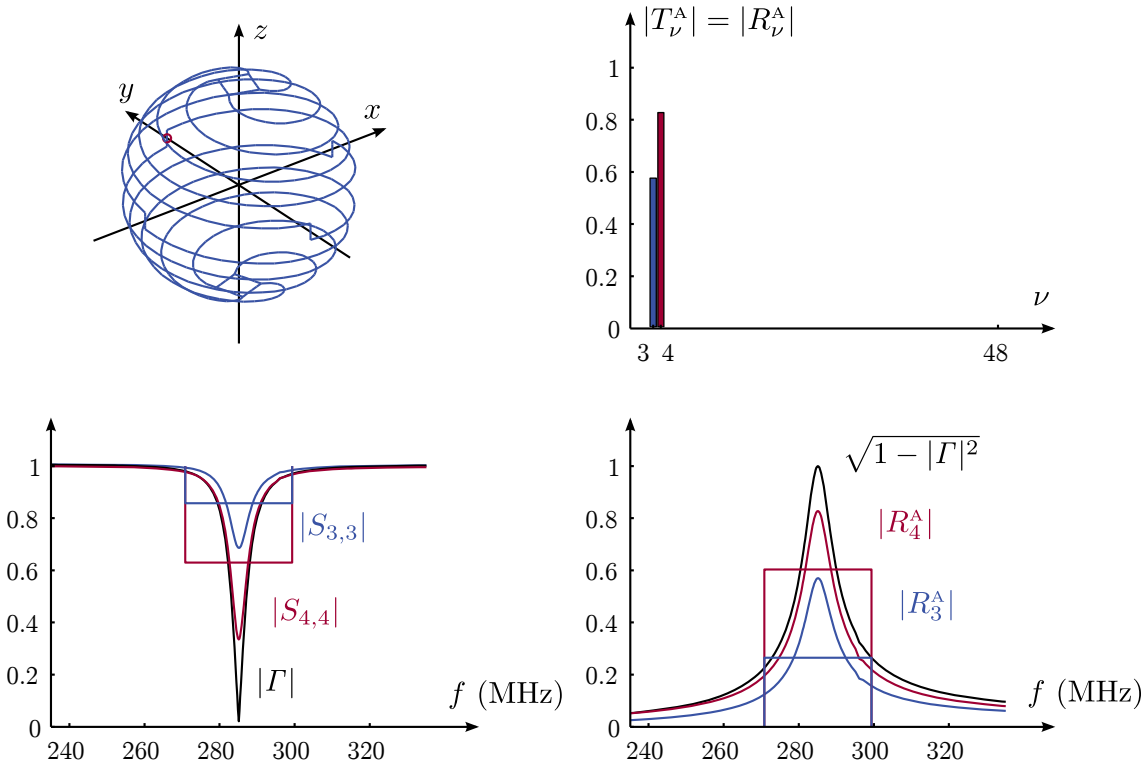

Figure 7: Upper left: The geometry of the elliptically polarized folded spherical helix (the red circle marks the location of the feed). Upper right: The moduli of the transmitting and receiving coefficients, $|T_\nu^{\mathrm{A}}| = |R_\nu^{\mathrm{A}}|$, at the resonance frequency $f = 285\,\mathrm{MHz}$. Lower left: Reflection coefficient Γ and scattering matrix elements $S_{3,3}$ and $S_{4,4}$ with the bound (3.4). Note that the bound on $S_{3,3}$ is tighter since $\nu = 3$ corresponds to a magnetic spherical wave (TE-mode), and the antenna is non-magnetic. Lower right: Square root of the mismatch $(1 - |\Gamma|^2)$, and receiving coefficients R_3^{A} and R_4^{A} with the bound (4.4).

antenna designs to illustrate the theoretical results of this paper.

All simulations have been done in the commercial software Efield (`http://www.efieldsolutions.com`). For all antennas, two separate simulations had to be carried out: In the first the antenna is transmitting, excited by a voltage source. This allows calculations of the antenna reflection coefficient Γ and the far-field $\boldsymbol{F}$. With the far-field, the spherical wave coefficients $d_\nu^{(1)}$ of the outgoing waves and the transmitting coefficients T_ν^{A} in (4.2) can be calculated, see Appendix A.2. The integral in (A.5) is solved numerically in Matlab. In the second simulation, the antenna is receiving: The voltage source is replaced by a load, and the antenna is excited with one regular spherical wave $\boldsymbol{v}_\nu$ at the time. The scattered far-field is calculated, and this in turn allows the coefficients of the outgoing waves $d_\nu^{(1)}$ and hence the scattering matrix elements $S_{\nu,\nu'}$ in (4.2) to be determined. The receiving coefficients R_ν^{A} are determined by calculating the power in the load. Recall that $R_\nu^{\mathrm{A}} = (-1)^s T_\nu^{\mathrm{A}}$ holds for a reciprocal antenna; this is a good error-check. With the procedure described here, the complete antenna scattering matrix $\mathbf{S}^{\mathrm{A}}$ in (4.1) can be determined.

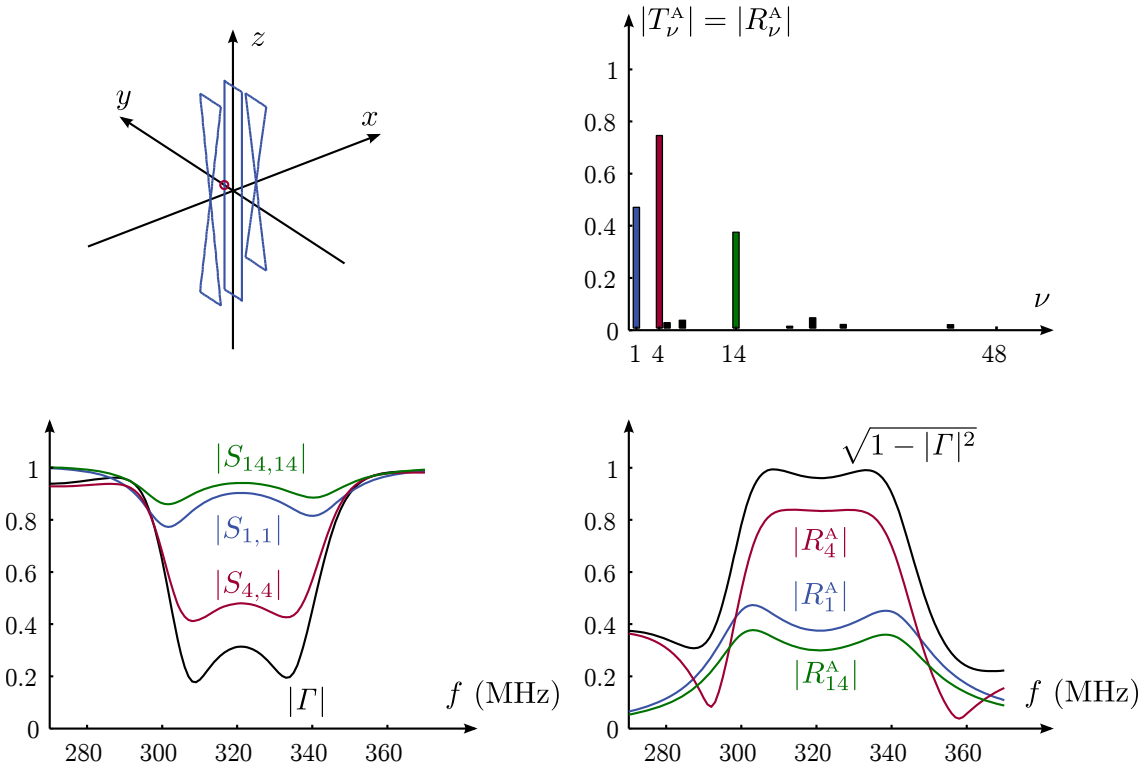

Figure 8: Upper left: The geometry of the directive Yagi-Uda antenna (the red circle marks the location of the feed). Upper right: The moduli of the transmitting and receiving coefficients, $|T^{\mathrm{A}}_\nu| = |R^{\mathrm{A}}_\nu|$, at the first resonance frequency $f = 304\,\mathrm{MHz}$. Lower left: Reflection coefficient Γ and scattering matrix elements $S_{1,1}$, $S_{4,4}$ and $S_{14,14}$. Lower right: Square root of the mismatch $(1 - |\Gamma|^2)$, and receiving coefficients R^{A}_1, R^{A}_4 and R^{A}_{14}.

To see the influence of the complex zeros k_n of $S_{\nu,\nu}$ in the sum rules (3.2), the integrals in the left hand sides as well as the static transition matrix elements appearing in the right hand sides have also been determined, see Table 1. The integrals were determined numerically over the finite frequency intervals in Figure 6 and Figure 7, respectively; this gives estimates from below, since all integrands are positive. The electrostatic transition matrix elements were calculated with an in-house Method of Moments code. Although only the results for the folded spherical helix antennas are included here, the static transition matrix elements of other antennas and higher order spherical waves can be determined in the same way. Note that the magnetostatic transition matrices vanish since the antennas are non-magnetic. The difference between the columns in Table 1 are due to the zeros k_n.

LP	$\frac{1}{\pi}\int_0^\infty \frac{1}{k^2} \ln \frac{1}{\lvert S_{4,4}(k)\rvert}\,\mathrm{d}k \geq 1.58\,\mathrm{mm}$	a	$= 41.8\,\mathrm{mm}$
	$\frac{1}{\pi}\int_0^\infty \frac{1}{k^4} \ln \frac{1}{\lvert S_{4,4}(k)\rvert}\,\mathrm{d}k \geq 40.2 \cdot 10^3\,\mathrm{mm}^3$	$c_1 T^{[2]}_{201,201}$	$= 42.7 \cdot 10^3\,\mathrm{mm}^3$
EP	$\frac{1}{\pi}\int_0^\infty \frac{1}{k^2} \ln \frac{1}{\lvert S_{3,3}(k)\rvert}\,\mathrm{d}k \geq 0.658\,\mathrm{mm}$	a	$= 41.8\,\mathrm{mm}$
	$\frac{1}{\pi}\int_0^\infty \frac{1}{k^4} \ln \frac{1}{\lvert S_{3,3}(k)\rvert}\,\mathrm{d}k \geq 18.3 \cdot 10^3\,\mathrm{mm}^3$	$c_1 T^{[1]}_{201,201}$	$= 0$
	$\frac{1}{\pi}\int_0^\infty \frac{1}{k^2} \ln \frac{1}{\lvert S_{4,4}(k)\rvert}\,\mathrm{d}k \geq 1.37\,\mathrm{mm}$	a	$= 41.8\,\mathrm{mm}$
	$\frac{1}{\pi}\int_0^\infty \frac{1}{k^4} \ln \frac{1}{\lvert S_{4,4}(k)\rvert}\,\mathrm{d}k \geq 38.4 \cdot 10^3\,\mathrm{mm}^3$	$c_1 T^{[2]}_{201,201}$	$= 41.4 \cdot 10^3\,\mathrm{mm}^3$

Table 1: The middle column presents the left hand sides of the applicable sum rules in (3.2) for the linearly and elliptically polarized folded spherical helix antennas in Figure 6 and Figure 7, respectively. The right column presents the respective right hand sides without the complex zeros k_n. The differences between the columns are due to the zeros.

5 Conclusion

The limitations (3.4) on the diagonal elements $S_{\nu,\nu}$ of the scattering matrix, which relate the coefficients of the incoming and outgoing vector spherical waves, were derived in this paper. The heterogeneous scatterer was assumed to be passive, with constitutive relations in convolution form in the time domain. The limitations state that the scattering matrix elements cannot be arbitrarily small over a whole wavenumber interval; the bound depends on the fractional bandwidth B, as well as the electrical size of the scatterer (wavenumber k times radius a of the circumscribing sphere) and its shape and static material properties (given by the electrostatic and magnetostatic transition matrix elements $T^{[\tau]}_{sml,sml}$). Specifically, it was seen that the order of the dominating term in the bandwidth bound for electrically small scatterers (Rayleigh scattering) increases with the order of the spherical wave, due to (3.5). A physical interpretation of the limitations (3.4) is that the absorption of power from each spherical wave is limited, as discussed in Section 3.2.

The derivations relied on a general approach for deriving sum rules and physical limitations for passive systems presented in [4], cf. also [3, 29]. A crucial intermediate result was the low-frequency asymptotic expansion (3.1) of the scattering matrix elements, which implied a set of sum rules, given by (3.2), from which the limitations (3.3) and (3.4) followed.

The limitations place bounds on the antenna scattering matrix $\mathbf{S}^{\mathrm{A}}$, given by (4.1). The limitations derived in the present paper are in form similar to the limitations on optimal broadband matching derived in [29, 38], although the interpretations are different, as discussed in Section 4.2. One advantage of the approach presented in this paper is that the limitations (3.4) incorporate the shape and static material properties of the antenna, and not just its electrical size as in [29, 38].

Finally, the antenna scattering matrix $\mathbf{S}^{\mathrm{A}}$ was calculated numerically for two folded spherical helix antennas and a directive Yagi-Uda antenna in Section 4.4. It was seen that the folded spherical helix antennas, which radiate dipole-patterns, performed close to the limitations. The electrically large Yagi-Uda antenna, with

directivity $D = 5.7$, had a quadrupole contribution in the far-field. Due to the limitations, such an antenna must be narrowband and/or electrically large.

Acknowledgment

The author would like to thank Mats Gustafsson and Henrik Gyllstad for truly helpful discussions during the work on this paper, and Mats Gustafsson also for his advice regarding some of the numerical computations. The financial support by the High Speed Wireless Communications Center of the Swedish Foundation for Strategic Research (SSF) is gratefully acknowledged.

Appendix A Details on vector spherical waves

The definitions of the incoming ($j = 2$) and outgoing ($j = 1$) vector spherical waves are those of Boström et al. [7], which only differs in normalization from those employed by Morse and Feshbach [28]:

$$\begin{cases} \boldsymbol{u}^{(j)}_{1sml}(k\boldsymbol{r}) = \mathrm{h}^{(j)}_l(kr)\boldsymbol{A}_{1sml}(\hat{\boldsymbol{r}}) = \dfrac{\nabla \times \boldsymbol{u}^{(j)}_{2sml}(k\boldsymbol{r})}{k}. \\ \boldsymbol{u}^{(j)}_{2sml}(k\boldsymbol{r}) = \dfrac{(kr\mathrm{h}^{(j)}_l(kr))'}{kr}\boldsymbol{A}_{2sml}(\hat{\boldsymbol{r}}) + \sqrt{l(l+1)}\dfrac{\mathrm{h}^{(j)}_l(kr)}{kr}\boldsymbol{A}_{3sml}(\hat{\boldsymbol{r}}) \\ \qquad\qquad = \dfrac{\nabla \times \boldsymbol{u}^{(j)}_{1sml}(k\boldsymbol{r})}{k}. \end{cases} \tag{A.1}$$

The same definitions are also used in [3], where more details can be found. Here $\mathrm{h}^{(j)}_l$ denotes the spherical Hankel function [2] of the j:th kind and order l, and a prime denotes differentiation with respect to the argument kr. The regular vector spherical waves $\boldsymbol{v}_\nu$ contain spherical Bessel functions j_l instead. The vector spherical harmonics $\boldsymbol{A}_{\tau sml}$ are defined by

$$\begin{cases} \boldsymbol{A}_{1sml}(\hat{\boldsymbol{r}}) = \dfrac{1}{\sqrt{l(l+1)}}\nabla \times (\boldsymbol{r}Y_{sml}(\hat{\boldsymbol{r}})) \\ \boldsymbol{A}_{2sml}(\hat{\boldsymbol{r}}) = \dfrac{1}{\sqrt{l(l+1)}}r\nabla Y_{sml}(\hat{\boldsymbol{r}}) \\ \boldsymbol{A}_{3sml}(\hat{\boldsymbol{r}}) = \hat{\boldsymbol{r}}Y_{sml}(\hat{\boldsymbol{r}}). \end{cases} \tag{A.2}$$

Here Y_{sml} are the (scalar) spherical harmonics

$$Y_{sml}(\theta,\phi) = \sqrt{\frac{2-\delta_{m0}}{2\pi}}\sqrt{\frac{2l+1}{2}\frac{(l-m)!}{(l+m)!}}P^m_l(\cos\theta)\left\{\begin{array}{c}\sin m\phi\\ \cos m\phi\end{array}\right\} \tag{A.3}$$

where $\delta_{mm'}$ denotes the Kronecker delta and P^m_l are associated Legendre polynomials [28]. The polar angle is denoted θ while ϕ is the azimuth angle. The upper (lower) expression is for $s = 1$ ($s = 2$), and the range of the indices are $l = 1, 2, \ldots$, $m = 0, 1, \ldots, l$, $s = 2$ when $m = 0$ and $s = 1, 2$ otherwise.

A.1 Low-frequency asymptotic expansion

To derive the low-frequency asymptotic expansion (2.5), consider the following low-frequency asymptotic expansion of the spherical Bessel and Hankel functions [2]:

$$\begin{cases} \mathrm{j}_l(z) = \dfrac{2^l l! z^l}{(2l+1)!} + \mathcal{O}(z^{l+2}) \\ \mathrm{h}_l^{(1)}(z) = -\mathrm{i}\dfrac{2l!}{2^l l! z^{l+1}} + \mathcal{O}(z^{-l+1}) \end{cases} \quad \text{as } z \to 0.$$

Inserting these into (A.1) gives

$$\begin{cases} \boldsymbol{v}_{2sml} = \dfrac{2^l (l+1)!}{(2l+1)!} k^{l-1} r^{l-1} \left[\boldsymbol{A}_{2sml}(\hat{\boldsymbol{r}}) + \sqrt{\dfrac{l}{l+1}} \boldsymbol{A}_{3sml}(\hat{\boldsymbol{r}}) \right] + \mathcal{O}(k^{l+1}) \\ \boldsymbol{u}_{2sml}^{(1)} = \dfrac{\mathrm{i}(2l)!}{2^l (l-1)!} k^{-l-2} r^{-l-2} \left[\boldsymbol{A}_{2sml}(\hat{\boldsymbol{r}}) - \sqrt{\dfrac{l+1}{l}} \boldsymbol{A}_{3sml}(\hat{\boldsymbol{r}}) \right] + \mathcal{O}(k^{-l}), \end{cases}$$

as $k \to 0$. Due to (A.2), this is equal to (2.5). In the same manner, it is straightforward to show that $\boldsymbol{v}_{1sml} = \mathcal{O}(k^l)$ and $\boldsymbol{u}_{1sml}^{(1)} = \mathcal{O}(k^{-l-1})$ as $k \to 0$.

A.2 Farfield to spherical wave coefficients

In the numerical simulations, there is a need to extract the coefficients of the outgoing spherical waves from a calculated far-field. The electric field of a transmitting antenna or the scattered field of a receiving antenna consists of only the outgoing spherical waves $\boldsymbol{u}^{(1)}$ in (2.3). In the far-field zone, this becomes

$$\boldsymbol{E}(\boldsymbol{r}) = \frac{\mathrm{e}^{\mathrm{i}kr}}{r} \left(1 + \mathcal{O}((kr)^{-1})\right) \underbrace{\sqrt{2\eta_0} \sum_{\nu} \mathrm{i}^{-l-2+\tau} d_\nu^{(1)} \boldsymbol{A}_\nu(\hat{\boldsymbol{r}})}_{\boldsymbol{F}(\hat{\boldsymbol{r}})} \quad \text{as } kr \to \infty, \tag{A.4}$$

where $\boldsymbol{F}$ is the far-field. Here the following expression was used [2]:

$$h_l^{(1)}(z) = \frac{\mathrm{e}^{\mathrm{i}z}}{\mathrm{i}^{l+1} z} \sum_{n=0}^{l} \frac{(l+n)!}{n!(l-n)!} (-2\mathrm{i}z)^{-n}.$$

The coefficients are given by [3]

$$d_\nu^{(1)} = \frac{\mathrm{i}^{l+2-\tau}}{\sqrt{2\eta_0}} \int_{\Omega_{\hat{\boldsymbol{r}}}} \boldsymbol{F}(\hat{\boldsymbol{r}}) \cdot \boldsymbol{A}_\nu(\hat{\boldsymbol{r}}) \, \mathrm{d}\Omega_{\hat{\boldsymbol{r}}}. \tag{A.5}$$

Appendix B More details on the static transition matrices

It was mentioned in Section 2.2 that the electrostatic and magnetostatic transition matrices for an uncharged scatterer can be seen as generalizations of the electric and

magnetic polarizability dyadics, defined in [23]. This statement is clarified here. The electric polarizability dyadic $\boldsymbol{\gamma}_{\mathrm{e}}$ relates the induced Cartesian electric dipole moment $\boldsymbol{p} = \int \boldsymbol{r}\rho(\boldsymbol{r})\,\mathrm{d}v$ in the scatterer to the applied electrostatic field $\boldsymbol{E}$ as $\boldsymbol{p} = \epsilon_0 \boldsymbol{\gamma}_{\mathrm{e}} \cdot \boldsymbol{E}$, where ϵ_0 denotes the permittivity of free space. Similarly, the magnetic polarizability dyadic $\boldsymbol{\gamma}_{\mathrm{m}}$ gives the induced Cartesian magnetic dipole moment $\boldsymbol{m} = \frac{1}{2}\int \boldsymbol{r}\times\boldsymbol{J}(\boldsymbol{r})\,\mathrm{d}v$ in the scatterer caused by an applied static magnetic field $\boldsymbol{H}$: $\boldsymbol{m} = \boldsymbol{\gamma}_{\mathrm{m}} \cdot \boldsymbol{H}$. Here the induced charge and current densities in the scatterer are denoted ρ and $\boldsymbol{J}$, respectively.

To see in what way the electrostatic transition matrix is a generalization of the polarizability dyadic, use the static free space Green's function to describe the scattered electrostatic potential [22]:

$$\phi(\boldsymbol{r}) = \frac{1}{\epsilon_0}\int \frac{\rho(\boldsymbol{r}')}{4\pi|\boldsymbol{r}-\boldsymbol{r}'|}\,\mathrm{d}v'.$$

The Green's function can be expanded into a sum of spherical harmonics; outside the sphere circumscribing the scatterer (where $r > r'$) it is [28, 31]

$$\frac{1}{4\pi|\boldsymbol{r}-\boldsymbol{r}'|} = \sum_{l=0}^{\infty}\sum_{m=0}^{l}\sum_{s=1}^{2}\frac{1}{2l+1}r'^{l}Y_{sml}(\hat{\boldsymbol{r}}')r^{-l-1}Y_{sml}(\hat{\boldsymbol{r}}).$$

Multiply $\phi(\boldsymbol{r})$ with $Y_{sml}(\hat{\boldsymbol{r}})$ and integrate over the unit sphere. This results in the following expressions for the coefficients $f^{(1)}_{sml}$ in (2.4):

$$f^{(1)}_{sml} = \frac{1}{\epsilon_0}\frac{1}{(2l+1)}p_{sml},$$

where the electric multipole moment is [28]

$$p_{sml} = \int r^l Y_{sml}(\hat{\boldsymbol{r}})\rho(\boldsymbol{r})\,\mathrm{d}v.$$

Consequently, a scatterer subject to the external potential

$$\phi(\boldsymbol{r}) = -r^{l'}Y_{s'm'l'}(\hat{\boldsymbol{r}})$$

gets an induced multipole moment given by [28]

$$p_{sml} = \epsilon_0(2l+1)T^{[2]}_{sml,s'm'l'}.$$

For the dipole case ($l = l' = 1$), this reduces to the relation [3]

$$T^{[2]}_{sm1,s'm'1} = \frac{1}{4\pi}\hat{\boldsymbol{n}}_{sm}\cdot\boldsymbol{\gamma}_{\mathrm{e}}\cdot\hat{\boldsymbol{n}}_{s'm'}.$$

where

$$\hat{\boldsymbol{n}}_{sm} = \begin{cases}\hat{\boldsymbol{x}}, & \text{for s=2, m=1}\\ \hat{\boldsymbol{y}}, & \text{for s=1, m=1}\\ \hat{\boldsymbol{z}}, & \text{for s=2, m=0}\end{cases}$$

and $\hat{\boldsymbol{x}}, \hat{\boldsymbol{y}}, \hat{\boldsymbol{z}}$ are the Cartesian unit vectors.

Likewise, an applied magnetostatic potential

$$\phi^{\mathrm{MS}}(\boldsymbol{r}) = -r^{l'} Y_{s'm'l'}(\hat{\boldsymbol{r}})$$

induces a magnetic multipole moment

$$m_{sml} = (2l+1) T^{[1]}_{sml,s'm'l'},$$

where [28]

$$m_{sml} = \frac{1}{l+1} \int (\boldsymbol{r} \times \boldsymbol{J}(\boldsymbol{r})) \cdot \nabla \left(r^l Y_{sml}(\boldsymbol{r}) \right) \mathrm{d}v.$$

The dipole case is [3]

$$T^{[1]}_{sm1,s'm'1} = \frac{1}{4\pi} \hat{\boldsymbol{n}}_{sm} \cdot \boldsymbol{\gamma}_{\mathrm{m}} \cdot \hat{\boldsymbol{n}}_{s'm'}.$$

References

[1] D. Arceo and C. A. Balanis. A compact Yagi-Uda antenna with enhanced bandwidth. *IEEE Antennas and Wireless Propagation Letters*, **10**, 442–445, 2011.

[2] G. B. Arfken and H. J. Weber. *Mathematical Methods for Physicists.* Academic Press, New York, fifth edition, 2001.

[3] A. Bernland, M. Gustafsson, and S. Nordebo. Physical limitations on the scattering of electromagnetic vector spherical waves. *J. Phys. A: Math. Theor.*, **44**(14), 145401, 2011.

[4] A. Bernland, A. Luger, and M. Gustafsson. Sum rules and constraints on passive systems. *J. Phys. A: Math. Theor.*, **44**(14), 145205, 2011.

[5] S. R. Best. Low Q electrically small linear and elliptical polarized spherical dipole antennas. *IEEE Trans. Antennas Propagat.*, **53**(3), 1047–1053, 2005.

[6] C. F. Bohren and D. R. Huffman. *Absorption and Scattering of Light by Small Particles.* John Wiley & Sons, New York, 1983.

[7] A. Boström, G. Kristensson, and S. Ström. Transformation properties of plane, spherical and cylindrical scalar and vector wave functions. In V. V. Varadan, A. Lakhtakia, and V. K. Varadan, editors, *Field Representations and Introduction to Scattering*, Acoustic, Electromagnetic and Elastic Wave Scattering, chapter 4, pages 165–210. Elsevier Science Publishers, Amsterdam, 1991.

[8] C. R. Brewitt-Taylor. Limitation on the bandwidth of artificial perfect magnetic conductor surfaces. *Microwaves, Antennas & Propagation, IET*, **1**(1), 255–260, 2007.

[9] L. J. Chu. Physical limitations of omni-directional antennas. *J. Appl. Phys.*, **19**, 1163–1175, 1948.

[10] R. E. Collin and S. Rothschild. Evaluation of antenna Q. *IEEE Trans. Antennas Propagat.*, **12**, 23–27, January 1964.

[11] R. M. Fano. Theoretical limitations on the broadband matching of arbitrary impedances. *Journal of the Franklin Institute*, **249**(1,2), 57–83 and 139–154, 1950.

[12] A. A. Glazunov, M. Gustafsson, A. Molisch, and F. Tufvesson. Physical modeling of multiple-input multiple-output antennas and channels by means of the spherical vector wave expansion. *IET Microwaves, Antennas & Propagation*, **4**(6), 778–791, 2010.

[13] M. Gustafsson and D. Sjöberg. Sum rules and physical bounds on passive metamaterials. *New Journal of Physics*, **12**, 043046, 2010.

[14] M. Gustafsson, C. Sohl, and G. Kristensson. Physical limitations on antennas of arbitrary shape. *Proc. R. Soc. A*, **463**, 2589–2607, 2007.

[15] M. Gustafsson, C. Sohl, and G. Kristensson. Illustrations of new physical bounds on linearly polarized antennas. *IEEE Trans. Antennas Propagat.*, **57**(5), 1319–1327, May 2009.

[16] M. Gustafsson and S. Nordebo. Bandwidth, Q factor, and resonance models of antennas. *Progress in Electromagnetics Research*, **62**, 1–20, 2006.

[17] M. Gustafsson and S. Nordebo. Characterization of MIMO antennas using spherical vector waves. *IEEE Trans. Antennas Propagat.*, **54**(9), 2679–2682, 2006.

[18] M. Gustafsson and D. Sjöberg. Physical bounds and sum rules for high-impedance surfaces. *IEEE Trans. Antennas Propagat.*, **59**(6), 2196–2204, 2011.

[19] J. E. Hansen, editor. *Spherical Near-Field Antenna Measurements*. Number 26 in IEE electromagnetic waves series. Peter Peregrinus Ltd., Stevenage, UK, 1988. ISBN: 0-86341-110-X.

[20] R. F. Harrington. *Time Harmonic Electromagnetic Fields*. McGraw-Hill, New York, 1961.

[21] A. Hujanen, J. Holmberg, and J. C.-E. Sten. Bandwidth limitations of impedance matched ideal dipoles. *IEEE Trans. Antennas Propagat.*, **53**(10), 3236–3239, 2005.

[22] J. D. Jackson. *Classical Electrodynamics*. John Wiley & Sons, New York, third edition, 1999.

[23] R. E. Kleinman and T. B. A. Senior. Rayleigh scattering. In V. V. Varadan and V. K. Varadan, editors, *Low and high frequency asymptotics*, volume 2 of *Handbook on Acoustic, Electromagnetic and Elastic Wave Scattering*, chapter 1, pages 1–70. Elsevier Science Publishers, Amsterdam, 1986.

[24] B. Kogan. Comments on "Broadband matching limitations for higher order spherical modes". *IEEE Trans. Antennas Propagat.*, **58**(5), 1826, 2010.

[25] P. A. Martin. *Multiple Scattering: Interaction of Time-Harmonic Waves with N Obstacles*, volume 107 of *Encyclopedia of Mathematics and its Applications*. Cambridge University Press, Cambridge, U.K., 2006.

[26] M. Migliore. On electromagnetics and information theory. *IEEE Trans. Antennas Propagat.*, **56**(10), 3188–3200, October 2008.

[27] M. I. Mishchenko, L. D. Travis, and D. W. Mackowski. T-matrix method and its applications to electromagnetic scattering by particles: A current perspective. *J. Quant. Spectrosc. Radiat. Transfer*, **111**(11), 1700–1703, 2010.

[28] P. M. Morse and H. Feshbach. *Methods of Theoretical Physics*, volume 2. McGraw-Hill, New York, 1953.

[29] S. Nordebo, A. Bernland, M. Gustafsson, C. Sohl, and G. Kristensson. On the relation between optimal wideband matching and scattering of spherical waves. *IEEE Trans. Antennas Propagat.*, **59**(9), 3358–3369, 2011.

[30] P. Olsson. Elastostatics as a limit of elastodynamics — a matrix formulation. *Applied Scientific Research*, **41**, 125–151, 1984.

[31] B. Peterson. Matrix formulation of static field problems involving an arbitrary number of bodies. *Inst. Theoretical Physics, S-412 96 Göteborg, Sweden*, **Report 75–12**, 1975.

[32] K. N. Rozanov. Ultimate thickness to bandwidth ratio of radar absorbers. *IEEE Trans. Antennas Propagat.*, **48**(8), 1230–1234, August 2000.

[33] D. Sjöberg. Variational principles for the static electric and magnetic polarizabilities of anisotropic media with perfect electric conductor inclusions. *J. Phys. A: Math. Theor.*, **42**, 335403, 2009.

[34] C. Sohl and M. Gustafsson. A priori estimates on the partial realized gain of Ultra-Wideband (UWB) antennas. *Quart. J. Mech. Appl. Math.*, **61**(3), 415–430, 2008.

[35] C. Sohl, M. Gustafsson, and G. Kristensson. Physical limitations on broadband scattering by heterogeneous obstacles. *J. Phys. A: Math. Theor.*, **40**, 11165–11182, 2007.

[36] J. Sten and A. Hujanen. Notes on the quality factor and bandwidth of radiating systems. *Electrical Engineering (Archiv fur Elektrotechnik)*, **84**(4), 189–195, 2002.

[37] J. A. Stratton. *Electromagnetic Theory*. McGraw-Hill, New York, 1941.

[38] M. C. Villalobos, H. D. Foltz, and J. S. McLean. Broadband matching limitations for higher order spherical modes. *IEEE Trans. Antennas Propagat.*, **57**(4), 1018–1026, 2009.

[39] J. Volakis, C. C. Chen, and K. Fujimoto. *Small Antennas: Miniaturization Techniques & Applications*. McGraw-Hill, New York, 2010.

[40] P. C. Waterman. The T-matrix revisited. *J. Opt. Soc. Am. A*, **24**(8), 2257–2267, Aug 2007.

[41] P. C. Waterman. T-matrix methods in acoustic scattering. *J. Acoust. Soc. Am.*, **125**(1), 42–51, 2009.

[42] P. C. Waterman. Matrix methods in potential theory and electromagnetic scattering. *J. Appl. Phys.*, **50**(7), 4550–4566, 1979.

[43] M. Wohlers and E. Beltrami. Distribution theory as the basis of generalized passive-network analysis. *IEEE Transactions on Circuit Theory*, **12**(2), 164–170, 1965.

[44] A. H. Zemanian. *Realizability theory for continuous linear systems*. Academic Press, New York, 1972.